




 Cite this: *RSC Adv.*, 2021, **11**, 24065

Sweetsop-like α -Fe₂O₃@CoNi catalyst with superior peroxidase-like activity for sensitive and selective detection of hydroquinone†

 Min Feng,^a Shaohua Wen,^a Xiaofang Chen,^a Die Deng,^a Xiupei Yang ^{*a} and Run Zhang ^{*b}

Hydroquinone (HQ) is poorly degradable in the ecological environment and is highly toxic to human health even at a low concentration. The colorimetric method has the advantages of low cost and fast analysis, which provides the possibility for simple and rapid detection of HQ. In this work, a new colorimetric method has been developed for HQ detection based on a peroxidase-like catalyst, α -Fe₂O₃@CoNi. This sweetsop-like α -Fe₂O₃@CoNi catalyst enables H₂O₂ to produce hydroxyl ([•]OH), leading to the oxidization of colorless 3,3',5,5'-tetramethylbenzidine (TMB) to blue oxTMB. In the presence of HQ, the blue oxTMB is reduced to colorless, which allows for colorimetric detection of HQ in water samples. This method has been validated by detecting HQ in water samples with high selectivity, rapid response, broad detection range (0.50 to 30 μ M), and low detection limit (0.16 μ M).

 Received 3rd May 2021
 Accepted 26th June 2021

DOI: 10.1039/d1ra03456a

rsc.li/rsc-advances

Introduction

Hydroquinone (1,4-dihydroxybenzene, HQ) is a phenolic compound widely used as an industrial reagent in cosmetics, dyes, plastics, textiles, rubber, medicine and other industries.^{1–3} During its industrial uses, the unavoidable contamination of the environment, especially water pollution, has threatened aquatic life.⁴ This compound is highly toxic to human health even at low concentrations and can cause damage to the skin, mouth, and respiratory system by inhalation.^{5–7} HQ is difficult to degrade in the ecological environment, and the accumulation of HQ caused by water discharge has always been a major environmental issue. HQ has been listed as a priority pollutant for aquatic environment monitoring by the US Environmental Protection Agency (EPA) and the European Union (EU).⁸ Therefore, HQ detection in water samples is essential for environmental regulation and human health. Currently, several methods have been developed for its detection, including electrochemiluminescence (ECL),^{9,10} high-performance liquid chromatography (HPLC),^{11,12} fluorometric method,^{13–15} gas chromatography-mass spectrometry (GC-MS),¹⁶ chemiluminescence (CL),^{17–19} etc. However, HQ detection by these methods can only be achieved in well-equipped laboratories

with the assistance of professional lab technicians, which makes them not suitable for quick and efficient determination of HQ in samples. In recent years, due to the convenience of the naked-eye colorimetric detection method, it is possible to easily and quickly visually inspect samples without any advanced equipment, which has gained considerable attention.^{20–22}

Natural enzymes have high substrate specificity and activity and are widely used in medicine, chemical industry, food processing, agriculture, detection, and other fields.^{23–25} However, the application of natural enzymes is fundamentally limited by their intrinsic drawbacks.^{26,27} Unlike natural enzymes, artificial nanozymes have obvious advantages such as high stability, low cost, and easy scale up.^{28,29} Therefore, artificial nanozyme can be an ideal candidate for various enzymatic reactions.^{30,31} Since the report of Fe₃O₄ nanoparticles' peroxidase activity in 2007, the preparation and application of nanozymes have aroused great interest among researchers.³² In the past 20 years, a number of nanomaterials have been developed and used as artificial enzymes.³³ These nanomaterials mainly include metal/metal oxide nanoparticles (NPs),³⁴ metal–organic frameworks (MOFs),³⁵ carbon nanomaterials,³⁶ etc. Iron oxide nanoparticles are one of the most typical nanoenzymes. They are widely used in biomedicine, biosensing and other fields due to their unique nanometer properties, stability and enzyme-like activity.³⁷ As an emerging class of artificial nanozymes, nanomaterials with peroxidase mimetic activity have also been widely used in the development of sensors for the detection of aqueous contaminants.^{38,39} Nevertheless, it remains interests to develop artificial nanozymes for rapid and effective colorimetric sensing of organic substrates, such as HQ, because the selection of

^aCollege of Chemistry and Chemical Engineering, Chemical Synthesis and Pollution Control Key Laboratory of Sichuan Province, China West Normal University, Nanchong 637000, China. E-mail: xiupeiyang@163.com

^bAustralian Institute for Bioengineering and Nanotechnology, The University of Queensland, Brisbane, Queensland 4072, Australia. E-mail: r.zhang@uq.edu.au

† Electronic supplementary information (ESI) available. See DOI: 10.1039/d1ra03456a



appropriate catalysts for oxidizing organic substrates to have colour changes is full of challenges.⁴⁰

In this work, we report the development of a new peroxidase-like catalyst, α -Fe₂O₃@CoNi, and its application for colorimetric detection of HQ in water samples. The sweetsop-like α -Fe₂O₃@CoNi was prepared by the one-pot hydrothermal method. The as-synthesized α -Fe₂O₃@CoNi showed high peroxidase activity, stability and was successfully applied to the colorimetric detection of HQ through catalytic oxidation with 3,3',5,5'-tetramethylbenzidine (TMB). The experimental results demonstrated that α -Fe₂O₃@CoNi could catalyze H₂O₂ to produce [•]OH which oxidized colorless TMB into blue oxTMB. The blue oxTMB be further reduced to TMB in the presence of HQ. Then a sensor for the colorimetric detection of HQ in water samples has been developed with α -Fe₂O₃@CoNi, H₂O₂ and TMB.

Experimental

Materials

Iron nitrate nonahydrate (Fe(NO₃)₃·9H₂O), Cobalt nitrate hexahydrate (Co(NO₃)₂·6H₂O), Ethylenediaminetetraacetic acid tetrasodium salt hydrate (Na₄EDTA·xH₂O), 3,3',5,5'-tetramethylbenzidine (TMB), hydroquinone (HQ), catechol, resorcinol, phenol, *o*-nitrophenol, *p*-nitrophenol, glucose and other nitrate salts including (Ca²⁺, Cu²⁺, Zn²⁺, Mg²⁺, Co²⁺, Mn²⁺, Cd²⁺, Fe³⁺, Cl⁻, SO₄²⁻, NO₃⁻) were purchased from Aladdin in China. Methanol, hydrogen peroxide (H₂O₂, 30%), Acetic acid (C₂H₄O₂), sodium acetate anhydrous (NaAc), nickel nitrate hexahydrate (Ni(NO₃)₂·6H₂O) were received from Chengdu Kelong Chemical Reagents Co. Ltd in China. The tap water and the river were collected from the laboratory and Jialing River of Nanchong, respectively.

Instrumentation

Transmission electron microscope (TEM) and mapping detected with an acceleration voltage of 200 kV on JEM-1200EX (JEOL, Tokyo, Japan). The scanning electron microscopy (SEM) and energy dispersive X-ray mappings (EDS) were performed on Hitachi S4800 (Hitachi Limited, Japan). X-ray photoelectron spectra (XPS) were obtained on a Thermo ESCALAB 250XI (Thermo Fisher Scientific, U.S.A.). The X-ray diffractometer (XRD) was measured using a Rigaku D/MAX-2550 (Rigaku, Japan) with Cu K α radiation. The infrared spectra were acquired from a Nicolet 6700 Fourier transform infrared (FTIR) spectrometer (Thermo Electron Corporation, USA) with a passed KBr pellet at room temperature. All absorption spectra were detected by a Shimadzu UV-2550 UV-vis absorption spectrophotometer (Kyoto, Japan). Electron spin resonance (ESR) spectra were recorded using Bruker MS-5000 ESR spectrometer (Bruker, Germany).

Preparation of α -Fe₂O₃@CoNi

Sweetsop-like α -Fe₂O₃@CoNi were prepared by previous one-pot hydrothermal method reported with some minor modifications.⁴¹ Briefly, a certain amount of EDTA was dissolved in

12 mL ultrapure water to form solution A. A certain amount of Fe(NO₃)₃·9H₂O, Co(NO₃)₂·6H₂O, Ni(NO₃)₂·6H₂O was dissolved in 8 mL ultrapure water to form a uniform mixture solution B. To solution A, solution B was slowly introduced under vigorously stirring. The resulting mixture was allowed to proceed for 10 minutes followed by the addition of 10 mL methanol. The aqueous solution obtained above was transferred to a Teflon-lined container and enclosed into a 100 mL stainless steel autoclave followed by heating at 180 °C for 12 h. After heating, the solution was cooled to room temperature and the solid sample was collected and dried under a vacuum after washing with ultrapure water. The product has a spherical shape with small particles on the surface, and its morphology is remarkably similar to that of sweetsop, so it was named as sweetsop-like α -Fe₂O₃@CoNi. Sweetsop is composed of many round or oval mature carpels connected together, and its aggregate berries are spherical or heart-shaped cones. Other single-metal composites (Co, Ni counterparts) were all fabricated through the same hydrothermal method as sweetsop-like α -Fe₂O₃@CoNi without adding the certain metal ions into solution B.

Peroxidase-like activity measurements and kinetic studies

The peroxidase-like catalytic activities of α -Fe₂O₃@CoNi nanozymes were investigated by the oxidation of TMB substrate in the presence of H₂O₂. All reactions were carried out in acetate buffer (0.20 M, pH = 6.0), and the absorbance at 652 nm was monitored using a UV-vis absorption spectrophotometer. The reactions were optimized under different α -Fe₂O₃@CoNi concentrations, TMB dosages, H₂O₂ dosages, reaction time, temperatures, type of buffer solution, buffer concentration and pH values. Use standard reaction conditions for steady-state kinetic determination, change the concentration of H₂O₂ (6.0–165.0 mM) at a fixed concentration of TMB (0.35 mM), and *vice versa*, change the concentration of TMB (0.25–2.5 mM) at a fixed concentration of H₂O₂ (130 mM). The Lineweaver–Burk plots is executed by the double reciprocal of the Michaelis–Menten equation to calculate the Michaelis constant (*K*_m) and the Maximum response speed (*V*_{max}).

Procedure for visual colorimetric determination of hydroquinone

Three milliliter of NaAc-HAc buffer (pH = 6.0), TMB (0.35 mM), H₂O₂ (30%, 40 μ L), α -Fe₂O₃@CoNi (3 mg mL⁻¹, 30 μ L) and the different concentrations of hydroquinone solution were added to a 4 mL spectrophotometer cell. The mixture was further incubated at 20 °C for 14 min followed by monitoring the formation of an oxidation product of TMB at 652 nm using UV-vis spectrophotometry. In order to investigate the selectivity of this colorimetric assay, hydroquinone was replaced by other materials, and the same experimental operations were also conducted. Subsequently, the content of hydroquinone water samples was evaluated according to the same steps described above, of which the samples of hydroquinone were prepared by spiking different concentrations of hydroquinone in real water samples.

Results and discussion

Preparation and characterization of α -Fe₂O₃@CoNi nanoparticles

Sweetsop-like α -Fe₂O₃@CoNi was prepared by the hydrothermal method, and the experimental conditions were optimized with temperatures, reaction times as well as the dosages of nitrate and EDTA (Fig. S1†). Fig. 1 shows the typical SEM image, TEM image, and element mapping images of sweetsop-like α -Fe₂O₃@CoNi. It clearly shows that α -Fe₂O₃@CoNi displays a uniformly spherical shape with a size of about 700 nm. The surface is covered by nanoparticles, like sweetsop (Fig. 1A) and confirmed by the TEM image (Fig. 1B). As shown in Fig. 1C–F, Fe, Co, Ni, and O are homogeneously dispersed in nanomaterials, which is consistent with EDS results (Fig. S2†). The marked diffraction peaks of crystalline α -Fe₂O₃@CoNi (Fig. 2A) are in good agreement with the well-established data (JCPDS 33-664). Sweetsop-like α -Fe₂O₃@CoNi, commercial Fe₂O₃ and EDTA were characterized using Fourier transform infrared (FT-IR) spectroscopy shown in Fig. S3.† It is proved that there are abundant hydrophilic groups on the surface of α -Fe₂O₃@CoNi, such as O–H (3400 cm⁻¹) and C=O (1600 cm⁻¹), which endow them with excellent water dispersibility. The IR peak at 586 cm⁻¹, can be attributed to the characteristic stretching vibration of the Fe–O bond.⁴² In addition, the absorption bands at 1340 cm⁻¹ identified the presence of C–N bonds from EDTA. To further confirm the chemical composition and surface state of α -Fe₂O₃@CoNi, XPS spectra were used to analyze the surface elemental composition (Fig. 2C–F). The full-range XPS spectrum further confirmed that the elemental components of α -Fe₂O₃@CoNi are Fe, Co, Ni, O, and C (Fig. 2C). In the high-resolution spectrum of Fe 2p (Fig. 2D), the two peaks located at 710.5 eV and 724.6 eV correspond to Fe 2p_{3/2} and Fe 2p_{1/2} respectively, and the energy difference is 14.1 eV, which corresponds to Fe³⁺ in α -Fe₂O₃@CoNi. As exhibited in Fig. 2E, two characteristic peaks at 781.0 and 796.9 eV are observed in the Co 2p spectrum, which link to 2p_{3/2} and 2p_{1/2} doublet of Co²⁺ and Co³⁺, respectively. Meanwhile, the Ni²⁺ was confirmed by the Ni

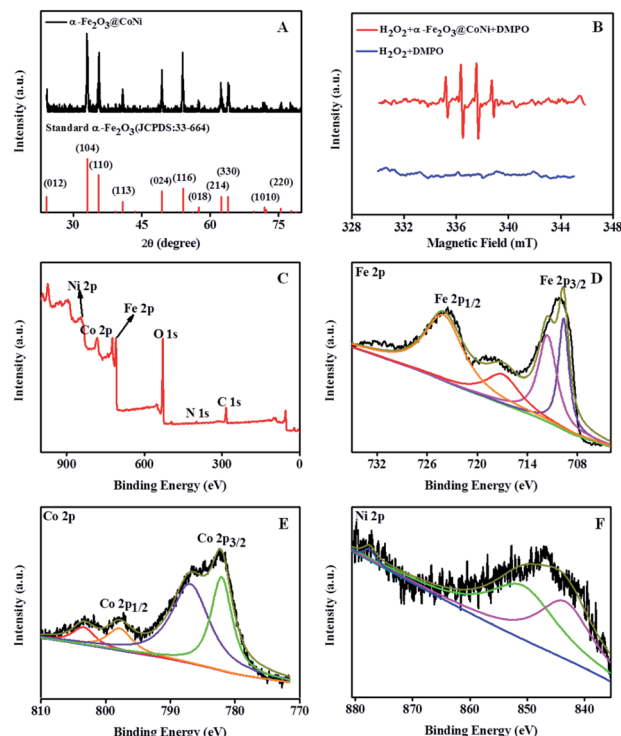


Fig. 2 (A) XRD pattern of α -Fe₂O₃@CoNi. (B) ESR spectra demonstrating \cdot OH generation by H₂O₂ and α -Fe₂O₃@CoNi + H₂O₂. XPS survey spectra of sweetsop-like α -Fe₂O₃@CoNi (C). Fe 2p, Co 2p and Ni 2p XPS spectra of α -Fe₂O₃@CoNi, respectively (D–F).

2p_{3/2} (852.3 eV) and Ni 2p_{1/2} (876 eV) peaks in α -Fe₂O₃@CoNi (Fig. 2F).⁴³ It further guaranteed that the Co and Ni on the surface of α -Fe₂O₃ were successfully immobilized.

Peroxidase-mimetic activity of α -Fe₂O₃@CoNi

The peroxidase-like activities of the four nanomaterials: commercial Fe₂O₃, α -Fe₂O₃@Co, α -Fe₂O₃@Ni, and α -Fe₂O₃@CoNi were studied by UV-vis absorption spectrum. After incubating α -Fe₂O₃@CoNi with TMB in a buffer solution containing H₂O₂ for 14 min, intense absorption bands centered at 652 nm (Fig. S4†) were observed and they were from the oxidation of TMB to oxTMB.^{44,45} The changes in solution from colorless to blue suggests the formation of oxTMB. In contrast, negligible changes of absorption spectra were observed after reacting of TMB with commercial Fe₂O₃, α -Fe₂O₃@Co and α -Fe₂O₃@Ni. The UV-vis data indicates that α -Fe₂O₃@CoNi has high catalytic activity for oxidation of TMB. At the same time, Fe₂O₃@Ni has a certain enzymatic activity, and the addition of Co adjusts the electronic structure to a certain extent, increases the electron transfer rate, and further improves its catalytic activity. The synergistic effect of Co, Ni, and α -Fe₂O₃ may be responsible for such high catalytic activity.

We then investigated the catalytic oxidation ability of α -Fe₂O₃@CoNi on the peroxidase substrate TMB to evaluate whether they can be applied as peroxidase mimics. As displayed in Fig. 3, TMB was oxidized to form a blue solution in the presence of H₂O₂ and α -Fe₂O₃@CoNi (inset in Fig. 3). A typical

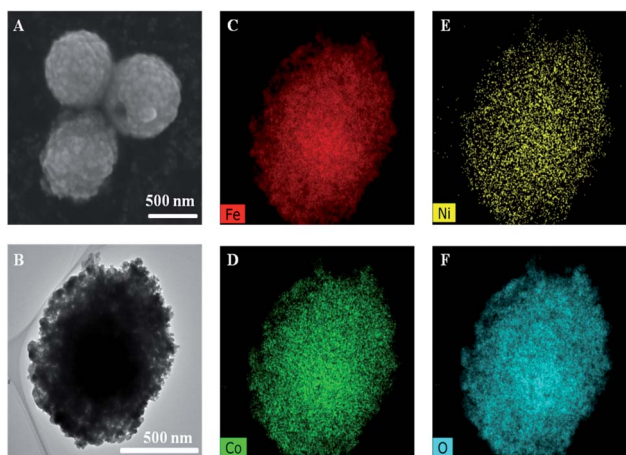


Fig. 1 The SEM (A), HRTEM (B) and element mapping images (C–F) of sweetsop-like α -Fe₂O₃@CoNi.

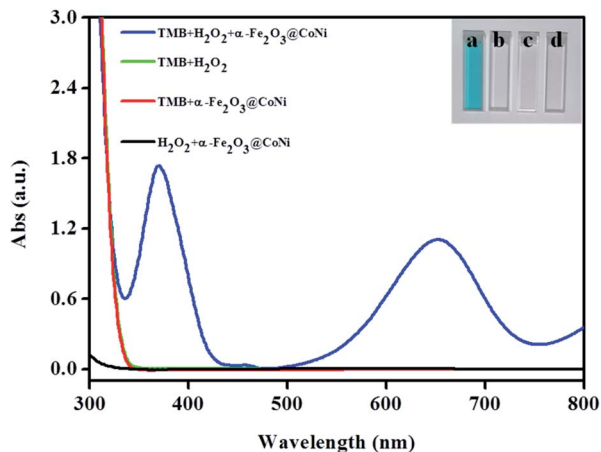


Fig. 3 Typical absorption spectra of the different solutions. (a) TMB + $\text{H}_2\text{O}_2 + \alpha\text{-Fe}_2\text{O}_3@ \text{CoNi}$, (b) TMB + H_2O_2 , (c) TMB + $\alpha\text{-Fe}_2\text{O}_3@ \text{CoNi}$, (d) $\text{H}_2\text{O}_2 + \alpha\text{-Fe}_2\text{O}_3@ \text{CoNi}$. Inset is the corresponding colorimetric photographs.

absorption peak of oxTMB centered at 652 nm (cuvette A in Fig. 3) was observed. Changes in UV-vis absorption spectra and solution color were not noticed for other groups, indicating that both H_2O_2 and $\alpha\text{-Fe}_2\text{O}_3@ \text{CoNi}$ are required for TMB oxidation. Similar to horseradish peroxidase (HRP), $\alpha\text{-Fe}_2\text{O}_3@ \text{CoNi}$ greatly enhanced the reaction of TMB with H_2O_2 , indicating that the $\alpha\text{-Fe}_2\text{O}_3@ \text{CoNi}$ can be considered as an efficient peroxidase mimic.

Effects of pH and temperature on $\alpha\text{-Fe}_2\text{O}_3@ \text{CoNi}$ -mediated catalytic oxidation were investigated and the results are shown in Fig. S5.† Obviously, the catalytic activity of $\text{Fe}_2\text{O}_3@ \text{CoNi}$ is dependent on pH and temperature. $\alpha\text{-Fe}_2\text{O}_3@ \text{CoNi}$ exhibits high catalytic activity at 20 °C and at pH 6 while others reported at 40–45 °C and at pH 4.5. Other experimental conditions on the catalytic oxidation of TMB in the $\alpha\text{-Fe}_2\text{O}_3@ \text{CoNi}/\text{H}_2\text{O}_2$ system were studied as well including the buffer solution (Fig. S6A and B†), the amount of $\alpha\text{-Fe}_2\text{O}_3@ \text{CoNi}$ (Fig. S6C†), the dosage of TMB (Fig. S6D†), and H_2O_2 (Fig. S6E†). The results suggested that the optimal conditions for catalytic oxidation of TMB were HAC-NaAc buffer (3 mL, pH 6), $\alpha\text{-Fe}_2\text{O}_3@ \text{CoNi}$ (30 μL , 3 mg mL^{-1}), TMB (70 μL , 15 mM), and H_2O_2 (40 μL , 30%).

Steady-state kinetics for $\alpha\text{-Fe}_2\text{O}_3@ \text{CoNi}$

In order to study the peroxidase-like activity of $\alpha\text{-Fe}_2\text{O}_3@ \text{CoNi}$, the apparent steady-state kinetic parameters of TMB oxidation were determined by changing the concentrations of H_2O_2 and TMB (Fig. 4), which is a similar strategy commonly used by HRP enzymes. Within the appropriate concentration range of H_2O_2 (Fig. 4A and B) and TMB (Fig. 4C and D), a typical Michaelis-Mentenlike curve was achieved. Based on the function of double-reciprocal Lineweaver–Burk plots ($1/V = K_m/V_{\text{max}} \times 1/[C] + 1/V_{\text{max}}$, where V_{max} is maximum response speed and K_m is an indicator of enzyme affinity toward its substrate. A lower K_m indicates the stronger affinity between enzymes and substrates),⁴⁶ Michaelis–Menten constant (K_m) was 0.23, 0.42 mM for TMB and H_2O_2 , respectively, and maximum initial

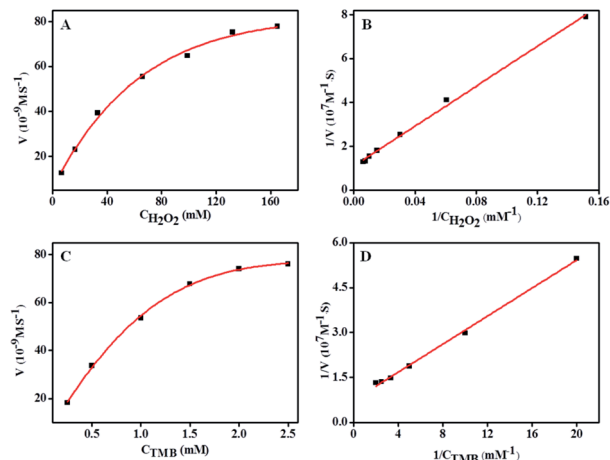


Fig. 4 Steady-state kinetic assay and catalytic mechanism of the reaction catalyzed by $\alpha\text{-Fe}_2\text{O}_3@ \text{CoNi}$. (A): TMB concentration was at 0.35 mM. (C): H_2O_2 concentration was at 130 mM. (B and D) Double-reciprocal Lineweaver–Burk plots of catalytic activity of $\alpha\text{-Fe}_2\text{O}_3@ \text{CoNi}$ with the same concentration of one substrate (TMB or H_2O_2) and the other varied.

velocity (V_{max}) was 13.5×10^{-8} and $9.3 \times 10^{-8} \text{ M s}^{-1}$ for TMB and H_2O_2 , respectively (Table S1†). As can be seen from the table, $\alpha\text{-Fe}_2\text{O}_3@ \text{CoNi}$ possesses smaller K_m and higher V_{max} than other nanozymes, indicating its outstanding peroxidase-like activity.

Selective and sensitive colorimetric detection of HQ

Fig. 5A and B show the time-dependent scanning kinetic curve and UV-Vis spectra of the $\alpha\text{-Fe}_2\text{O}_3@ \text{CoNi}$ in TMB/ H_2O_2 system at different HQ dosages. The absorbance at 652 nm decreased significantly with the increasing HQ concentration, indicating that HQ successfully inhibited the oxidation of TMB. As shown in Fig. 5C, UV-vis absorption of the solution containing TMB,

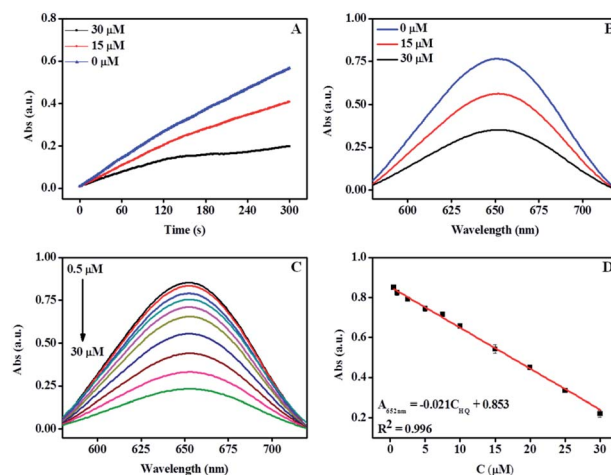


Fig. 5 The Time-dynamics scanning spectrum (A) and the absorption spectra (B) of TMB + $\text{H}_2\text{O}_2 + \alpha\text{-Fe}_2\text{O}_3@ \text{CoNi}$ system with different concentrations of HQ. (C) The absorption spectra of oxTMB with different HQ concentrations. (D) The linear calibration plot for HQ.

H_2O_2 , and $\alpha\text{-Fe}_2\text{O}_3\text{@CoNi}$ were gradually reduced upon the addition of HQ. A good linear relationship ($R^2 = 0.996$) was obtained when plotting the absorbance at 652 nm against the HQ concentration range of 0.50–30 μM . The detection limit 0.16 μM (0.018 mg L^{-1}) is lower than the U.S. Environment Protection Agency estimated wastewater discharge limit of 0.5 mg L^{-1} . Compared with other methods (Table S2†), our approach has a higher sensitivity for HQ detection. The selective response of the proposed method for HQ detection over other ions and molecules was evaluated in the aqueous solutions containing TMB, H_2O_2 and $\alpha\text{-Fe}_2\text{O}_3\text{@CoNi}$, 20-fold of potential interference species, including Fe^{3+} , Cd^{2+} , Ca^{2+} , Mn^{2+} , Mg^{2+} , Cu^{2+} , Co^{2+} , Zn^{2+} , Cl^- , SO_4^{2-} , NO_3^- , glucose, catechol, resorcinol, phenol, *o*-nitrophenol, *p*-nitrophenol, and glycine. Changes of the UV-vis absorbance ($(A_0 - A)/A_0$) were determined after 1 min incubation and presented in Fig. 6. As shown in Fig. 6, no significant changes in $(A_0 - A)/A_0$ were observed upon the addition of ions and molecules except HQ. Catechol has a similar structure to hydroquinone, which might interfere the HQ detection (Fig. S7†). The interference from catechol may be minimized by using activated alumina as it has been reported that activated alumina can adsorb catechol. The optimum amount of alumina used was explored to not interfere with the detection of HQ while adsorbing catechol and the results are shown in Fig. S8.†

Further understanding of the detection mechanism

According to previous reports, the catalytic mechanism of nanozymes can be divided into two categories: one is the transfer of electrons between the substrate and H_2O_2 , and the other is the active substance in the catalytic system.^{38,47} In order to study the catalytic mechanism, isopropanol (IPA) was added to the solution containing TMB, H_2O_2 , and $\alpha\text{-Fe}_2\text{O}_3\text{@CoNi}$. As a hydroxyl radical scavenger, IPA was often used to detect hydroxyl radicals in the oxidation process.⁴⁸ As shown in Fig. S9,† the absorption at 652 nm is significantly reduced after adding IPA (10 mM), which proves the generation of hydroxyl

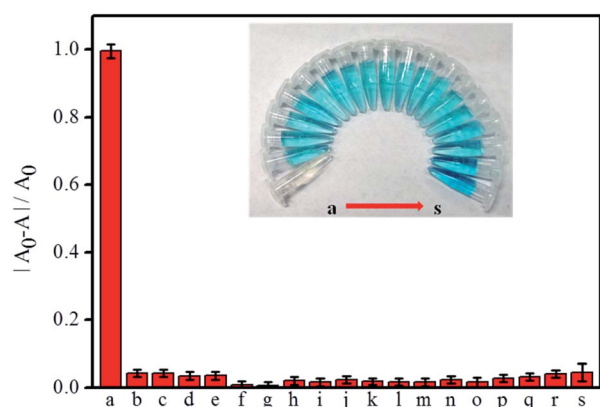


Fig. 6 Effect of several metal ions and molecules on the chromogenic system and corresponding photograph (inset). From a to s are hydroquinone, glycine, resorcinol, catechol, phenol, *o*-nitrophenol, *p*-nitrophenol, glucose, Zn^{2+} , Co^{2+} , Cu^{2+} , Mg^{2+} , Mn^{2+} , Cl^- , SO_4^{2-} , NO_3^- , Ca^{2+} , Cd^{2+} , Fe^{3+} , respectively.

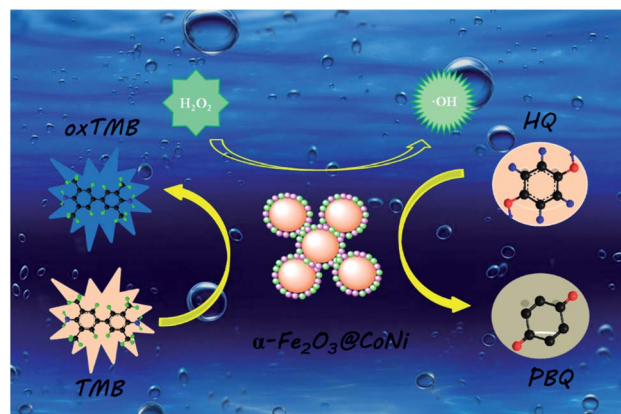


Fig. 7 Colorimetric sensing mechanism of HQ.

Table 1 Analytical results of the HQ determination in spiked samples

Sample	Added (μM)	Found (μM)	Recovery (%)	RSD (% , $n = 5$)
Tap water	2.50	2.57 ± 0.08	102.8%	1.75
	7.50	6.85 ± 0.06	91.3%	1.75
	22.50	21.07 ± 0.02	93.6%	4.60
Jialing water	2.50	2.53 ± 0.09	101.2%	4.94
	7.50	7.27 ± 0.03	96.9%	3.63
	22.50	22.44 ± 0.01	99.7%	4.47

radicals ($\cdot\text{OH}$). At the same time, electron spin resonance (ESR) spectroscopy is used to explore the reaction mechanism and the active free radicals generated during the reaction. As shown in Fig. 2B, a characteristic signal peak of DMPO- $\text{HO}\cdot$ with an intensity of 1 : 2 : 2 : 1 was generated after the addition of $\alpha\text{-Fe}_2\text{O}_3\text{@CoNi}$, indicating that $\alpha\text{-Fe}_2\text{O}_3\text{@CoNi}$ can catalyze H_2O_2 to produce $\cdot\text{OH}$.⁴⁹ Based on the experimental results and previous reports, the mechanism of the peroxide-like activity of $\alpha\text{-Fe}_2\text{O}_3\text{@CoNi}$ was proposed and illustrated in Fig. 7. H_2O_2 is first adsorbed on the surface of $\alpha\text{-Fe}_2\text{O}_3\text{@CoNi}$, and then $\alpha\text{-Fe}_2\text{O}_3\text{@CoNi}$ promotes the decomposition of H_2O_2 to produce $\cdot\text{OH}$, which can further oxidize TMB and produce blue substances. The addition of HQ reduces oxTMB to TMB, which is oxidized to *p*-benzoquinone.

Determination of HQ in real samples

To validate the feasibility of the proposed method for HQ colorimetric detection in tap water and river water, HQ was spiked into them, and the concentration of HQ was measured thereafter. As shown in Table 1, the recoveries of HQ in spiked samples were in the range of 91.3–102.8%, with RSDs <5%. Such results demonstrated that the proposed method has good accuracy and precision for HQ detection in spiked water samples.

Conclusions

Sweetsop-like $\alpha\text{-Fe}_2\text{O}_3\text{@CoNi}$ prepared by hydrothermal method was characterized by SEM, TEM, XRD, and XPS. An

efficient and convenient HQ quantitative detection method was developed based on the peroxidase-like activity of $\alpha\text{-Fe}_2\text{O}_3\text{@-CoNi}$. This developed colorimetric method for HQ detection exhibited high sensitivity (detection limit 0.16 μM) and selectivity and was validated *via* spiked water samples.

Conflicts of interest

There are no conflicts to declare.

Acknowledgements

This work was financially supported by the National Natural Science Foundation of China (21777130, 41807210), the Natural Science Foundation of Sichuan Province of China (2019YJ0522, 2018JY0184), the Meritocracy Research Funds of China West Normal University (463132) and the Fundamental Research Funds of China West Normal University (416390).

Notes and references

- 1 R. Li, Z. Li, G. Wang and Z. Gu, *Sens. Actuators, B*, 2018, **276**, 404–412.
- 2 J. Ahmed, M. M. Rahman, I. A. Siddiquey, A. M. Asiri and M. A. Hasnat, *Sens. Actuators, B*, 2018, **256**, 383–392.
- 3 Y. Wee, S. Park, Y. H. Kwon, Y. Ju, K. M. Yeon and J. Kim, *Biosens. Bioelectron.*, 2019, **132**, 279–285.
- 4 H. Wang, Q. Hu, Y. Meng, Z. Jin, Z. Fang, Q. Fu, W. Gao, L. Xu, Y. Song and F. Lu, *J. Hazard. Mater.*, 2018, **353**, 151–157.
- 5 H. Wang, R. Li and Z. Li, *Electrochim. Acta*, 2017, **255**, 323–334.
- 6 Y. Liu, Q. Wang, S. Guo, P. Jia, Y. Shui, S. Yao, C. Huang, M. Zhang and L. Wang, *Sens. Actuators, B*, 2018, **275**, 415–421.
- 7 C. Lou, T. Jing, J. Zhou, J. Tian, Y. Zheng, C. Wang, Z. Zhao, J. Lin, H. Liu, C. Zhao and Z. Guo, *Int. J. Biol. Macromol.*, 2020, **149**, 1130–1138.
- 8 D. Balram, K. Y. Lian and N. Sebastian, *Ultrason. Sonochem.*, 2019, **58**, 104650–104673.
- 9 D. L. Huang, J. Wang, F. Cheng, A. Ali, H. S. Guo, X. Ying, L. P. Si and H. Y. Liu, *Microchim. Acta*, 2019, **186**, 381–392.
- 10 R. Huang, D. Liao, S. Chen, J. Yu and X. Jiang, *Sens. Actuators, B*, 2020, **320**, 128386–128395.
- 11 D. Cheaib, N. El Darra, H. N. Rajha, I. El-Ghazzawi, Y. Mounemne, A. Jammoul, R. G. Maroun and N. Louka, *Antioxidants*, 2018, **7**, 174–186.
- 12 Q. Zhou, M. Lei, Y. Wu, X. Zhou, H. Wang, Y. Sun, X. Sheng and Y. Tong, *Chemosphere*, 2020, **238**, 124621–124627.
- 13 Y. Wang, Q. Yue, L. Tao, C. Zhang and C. Z. Li, *Microchim. Acta*, 2018, **185**, 550–559.
- 14 X. Wang, Z. Cheng, Y. Zhou, S. K. Tammina and Y. Yang, *Microchim. Acta*, 2020, **187**, 350–358.
- 15 Y. Liu, Y. Cao, T. Bu, X. Sun, T. Zhe, C. Huang, S. Yao and L. Wang, *Microchim. Acta*, 2019, **186**, 399–407.
- 16 Q. Ye, F. Yan, D. Kong, J. Zhang, X. Zhou, J. Xu and L. Chen, *Sens. Actuators, B*, 2017, **250**, 712–720.
- 17 Y. Chao, X. Zhang, L. Liu, L. Tian, M. Pei and W. Cao, *Microchim. Acta*, 2014, **182**, 943–948.
- 18 S. Xu, J. Li, X. Li, M. Su, Z. Shi, Y. Zeng and S. Ni, *Microchim. Acta*, 2015, **183**, 667–673.
- 19 Z. Y. Lin, Y. C. Kuo, C. J. Chang, Y. S. Lin, T. C. Chiu and C. C. Hu, *RSC Adv.*, 2018, **8**, 19381–19388.
- 20 H. Yang, M. Xiao, W. Lai, Y. Wan, L. Li and H. Pei, *Anal. Chem.*, 2020, **92**, 4990–4995.
- 21 Z. Gao, G. G. Liu, H. Ye, R. Rauschendorfer, D. Tang and X. Xia, *Anal. Chem.*, 2017, **89**, 3622–3629.
- 22 L. Zhi, X. Zeng, H. Wang, J. Hai, X. Yang, B. Wang and Y. Zhu, *Anal. Chem.*, 2017, **89**, 7649–7658.
- 23 N. Luo, Z. Yang, F. Tang, D. Wang, M. Feng, X. Liao and X. Yang, *ACS Appl. Nano Mater.*, 2019, **2**, 3951–3959.
- 24 L. Zhang, X. Hai, C. Xia, X. W. Chen and J. H. Wang, *Sens. Actuators, B*, 2017, **248**, 374–384.
- 25 X. Li, J. Li, J. Zhu, S. Hao, G. Fang, J. Liu and S. Wang, *Chem. Commun.*, 2019, **55**, 13458–13461.
- 26 F. Tian, J. Zhou, B. Jiao and Y. He, *Nanoscale*, 2019, **11**, 9547–9555.
- 27 X. Wang, L. Qin, M. Lin, H. Xing and H. Wei, *Anal. Chem.*, 2019, **91**, 10648–10656.
- 28 Y. Liu, H. Jin, W. Zou and R. Guo, *RSC Adv.*, 2020, **10**, 28819–28826.
- 29 X. Wang, L. Qin, M. Zhou, Z. Lou and H. Wei, *Anal. Chem.*, 2018, **90**, 11696–11702.
- 30 M. Liang, Y. Wang, K. Ma, S. Yu, Y. Chen, Z. Deng, Y. Liu and F. Wang, *Small*, 2020, **16**, 2002348–2002357.
- 31 M. Liang and X. Yan, *Acc. Chem. Res.*, 2019, **52**, 2190–2200.
- 32 L. Gao, J. Zhuang, L. Nie, J. Zhang, Y. Zhang, N. Gu, T. Wang, J. Feng, D. Yang, S. Perrett and X. Yan, *Nat. Nanotechnol.*, 2007, **2**, 577–583.
- 33 B. Liu and J. Liu, *Nano Res.*, 2017, **10**, 1125–1148.
- 34 X. Shen, W. Liu, X. Gao, Z. Lu, X. Wu and X. Gao, *J. Am. Chem. Soc.*, 2015, **137**, 15882–15891.
- 35 C. Huang, J. Dong, W. Sun, Z. Xue, J. Ma, L. Zheng, C. Liu, X. Li, K. Zhou, X. Qiao, Q. Song, W. Ma, L. Zhang, Z. Lin and T. Wang, *Nat. Commun.*, 2019, **10**, 2779–2789.
- 36 X. Qu, H. Sun, Y. Zhou and J. Ren, *Angew. Chem., Int. Ed.*, 2018, **57**, 9224–9237.
- 37 L. Gao, K. Fan and X. Yan, *Theranostics*, 2017, **7**, 3207–3227.
- 38 S. Zhang, D. Zhang, X. Zhang, D. Shang, Z. Xue, D. Shan and X. Lu, *Anal. Chem.*, 2017, **89**, 3538–3544.
- 39 L. Zhi, W. Zuo, F. Chen and B. Wang, *ACS Sustainable Chem. Eng.*, 2016, **4**, 3398–3408.
- 40 X. Wang, M. Zhao, Y. Song, Q. Liu, Y. Zhang, Y. Zhuang and S. Chen, *Sens. Actuators, B*, 2019, **283**, 130–137.
- 41 Q. Zhang, N. M. Bedford, J. Pan, X. Lu and R. Amal, *Adv. Energy Mater.*, 2019, **9**, 1901312–1901325.
- 42 O. F. Odio, L. Lartundo-Rojas, P. Santiago-Jacinto, R. Martínez and E. Reguera, *J. Phys. Chem. C*, 2014, **118**, 2776–2791.
- 43 L. Yang, D. Wang, Y. Lv and D. Cao, *Carbon*, 2019, **144**, 8–14.
- 44 M. K. Masud, S. Yadav, M. N. Islam, N. T. Nguyen, C. Salomon, R. Kline, H. R. Alamri, Z. A. Allothman, Y. Yamauchi, M. S. A. Hossain and M. J. A. Shiddiky, *Anal. Chem.*, 2017, **89**, 11005–11013.

- 45 D. Yi, Z. Wei, W. Zheng, Y. Pan, Y. Long and H. Zheng, *Sens. Actuators, B*, 2020, **323**, 128691–128697.
- 46 M. Ivanova, E. Grayfer, E. Plotnikova, L. Kibis, G. Darabdhara, P. Boruah, M. Das and V. Fedorov, *ACS Appl. Mater. Interfaces*, 2019, 22102–22112.
- 47 J. Liang, H. Li, J. Wang, H. Yu and Y. He, *Anal. Chem.*, 2020, **92**, 6548–6554.
- 48 L. Jiao, J. Wu, H. Zhong, Y. Zhang, W. Xu, Y. Wu, Y. Chen, H. Yan, Q. Zhang, W. Gu, L. Gu, S. P. Beckman, L. Huang and C. Zhu, *ACS Catal.*, 2020, **10**, 6422–6429.
- 49 X. Huang, F. Xia and Z. Nan, *ACS Appl. Mater. Interfaces*, 2020, **12**, 46539–46548.